Advective transport of CO_2 in permeable media induced by atmospheric pressure fluctuations: 1. An analytical model

W. J. Massman[1]

Received 13 January 2006; revised 12 April 2006; accepted 18 May 2006; published 28 July 2006.

[1] Advective flows within soils and snowpacks caused by pressure fluctuations at the upper surface of either medium can significantly influence the exchange rate of many trace gases from the underlying substrate to the atmosphere. Given the importance of many of these trace gases in understanding biogeochemical cycling and global change, it is crucial to quantify (as much as possible) any impact these flows can have on the transport of these gases. This study (part 1 of 2) details a new model describing the influence that naturally occurring, pressure-driven, oscillatory advective flows have on CO_2 profiles within soils and snowpacks and on the associated CO_2 fluxes emanating from the underlying source. This model, which consists of two layers with differing permeability and CO_2 source strength, is developed for both a dispersive and a nondispersive medium. The pressure forcing and the CO_2 response, modeled as plane waves in time and the horizontal direction, have amplitudes that vary in the vertical direction as described by analytical solutions to the diffusion equation (for pressure) and the advective-diffusive and dispersive-diffusive equations (for CO_2). In the case of a dispersive medium, the dispersion coefficient is derived in terms of the horizontal wave number and amplitude of the pressure forcing at the upper surface and the vertical structure and dispersivity of the medium. Diffusive flux enhancement factors, developed for the dispersive and nondispersive models, are expressed as functions of the surface amplitude of the pressure forcing, the permeability and cross-sectional shape and dimension of the pore tubes of the medium, and the vertical structure of the medium. Results indicate that advective flows induced by naturally occurring atmospheric pressure fluctuations are likely to enhance diffusive fluxes more in a dispersive medium than a nondispersive medium. However, such pressure forcing can significantly enhance diffusive fluxes in either medium.

Citation: Massman, W. J. (2006), Advective transport of CO_2 in permeable media induced by atmospheric pressure fluctuations: 1. An analytical model, *J. Geophys. Res.*, *111*, G03004, doi:10.1029/2006JG000163.

1. Introduction

[2] Given the increasing concern about the buildup of trace gases in the atmosphere and their possible influence on global change and atmospheric chemistry, it is important to understand the physical processes that control their exchange between the atmosphere and the biosphere. For soil-atmosphere gas exchange, molecular diffusion is a key process in virtually all situations. However, over a century ago, *Buckingham* [1904] proposed that naturally occurring advective flows in soils induced by variations in atmospheric pressure at the soil's surface might also affect the exchange of gases between the soil and the atmosphere. This pressure-related phenomenon, which has been termed wind pumping, atmospheric (pressure) pumping, and barometric pumping [*Fukuda*, 1955; *Colbeck*, 1989; *Nilson et al.*, 1991; *Auer et al.*, 1996], occurs not only in soils but in any permeable medium exposed to a time-varying pressure field or a static pressure differential. There are many natural settings where these types of pressure forcing can occur.

[3] For example, whenever moving air or any moving fluid encounters an obstacle, a static pressure differential is formed between the windward and leeward sides of the obstacle. If the obstacle is permeable, then the fluid, which will be forced through it as a result of the pressure difference, will transport material through the obstacle. Similarly, any time-varying or periodic pressure field at the top of a permeable layer (soils, snowpacks, benthic sediments) will induce periodic motions within the medium [e.g., *Waddington et al.*, 1996]. In this case, however, these periodic motions are not simple symmetric motions, which would just move fluid back and forth with no net transport. Rather, within the pore spaces and connecting paths of the permeable medium, these oscillatory flows asymmetrically enhance the diffusional exchange through both shear dis-

[1]Rocky Mountain Research Station, USDA Forest Service, Fort Collins, Colorado, USA.

persion, caused by viscous drag at the pore boundaries [*Watson*, 1983], and rotational dispersion, which occurs when the direction of the pressure gradient rotates with time [*Webster and Taylor*, 1992].

[4] In the broadest sense, these two pressure-related processes epitomize the two major physical processes associated with naturally occurring pressure-induced exchange at the Earth's surface: a moving fluid interacting with a rough surface, which will induce pressure fields associated with drag, and the existence or persistence over the surface of a permeable medium of either a stationary or a propagating pressure field caused by some remote phenomenon. Although these physical transport processes may be relatively few, there are a great variety of physical phenomena associated with variations in surface pressure. Among them are high-frequency atmospheric turbulence, which can be characterized by timescales between about 10^{-1} s and about 10^3 s and space scales between about 10^{-2} m and 10^2 m [*Colbeck*, 1989; *Massman et al.*, 1997], and low-frequency synoptic-scale atmospheric motions, which have wavelengths of about 10^6 m and periods of a week or so ($\approx 10^6$ s) [*Massmann and Farrier*, 1992; *Auer et al.*, 1996]. Between these extremes lie atmospheric gravity waves [*Nappo*, 2002; *Lee and Barr*, 1998], solitary waves [*Hauf et al.*, 1996; *Rees et al.*, 1998], mesoscale disturbances [*Grivet-Talocia et al.*, 1999], coherent turbulent structures within the atmospheric surface layer [*Katul et al.*, 1997; *Watanabe*, 2004], and a host of other phenomena, all of which can cause natural pressure-induced advective flows in soils.

[5] Because of the ubiquity of these natural flows and the permeable nature of most of the Earth's surface, pressure-induced advective flows have been studied in a variety of settings, some of which include: the transport of heat, trace gas, and aerosols in snowpacks and glacial firn [*Gjessing*, 1977; *Albert and McGilvary*, 1992; *Cunningham and Waddington*, 1993; *Massman et al.*, 1997; *Albert and Hardy*, 1995], dating trace gases held within sand dunes [*Severinghaus et al.*, 1997], radon entry into basements [*Robinson et al.*, 1997], CO_2 profiles along geological faults [*Lewicki et al.*, 2003], and the exchange of nutrients and solutes within benthic sediment layers in coastal regions [*Harrison et al.*, 1983; *Huettel and Webster*, 2001; *Jiao and Li*, 2004].

[6] While it does appear that naturally occurring pressure-induced advective flows are common, their importance to gas transfer relative to diffusion can vary significantly. For oscillatory flows with high Schmidt number (*Sc*), transport by these natural advective motions can dominate diffusion [*Watson*, 1983; *Webster*, 2003]. When $Sc \approx 1$ or less, however, the pressure-induced transport is likely to be small compared to diffusion [*Waddington et al.*, 1996] or at least to contribute much less to transport than the high *Sc* oscillatory flows [*Watson*, 1983]. Other studies [e.g., *Colbeck*, 1989] suggest that standing or stationary pressure waves or a stationary pressure differential (like that forced by flow over irregular topography) are more effective at pressure-induced transport than traveling waves (like those associated with atmospheric turbulence) and that stationary waves have the potential to enhance diffusion significantly. It has also been suggested that low-frequency atmospheric motions are less effective than higher-frequency motions at trace gas transport [*Waddington et al.*, 1996]. Finally, flows forced by natural pressure variations in a dispersive medium can be considerably more efficient at trace gas transport than similar flows in a nondispersive medium [*Scotter and Raats*, 1968; *Auer et al.*, 1996].

[7] The purpose of this work (part 1) is to outline a new (physically based) analytical model describing natural pressure-induced advective flows in snowpacks and soils and their impact on CO_2 profiles and the associated diffusional flux enhancements. The model, developed for both dispersive and nondispersive media, consists of two layers with differing permeability and CO_2 source strength. The pressure forcing and the CO_2 response, represented as linear plane waves in time and in the horizontal direction, have amplitudes that vary with depth in accordance with analytical solutions to the diffusive and advective-diffusive equations. The complete CO_2 profile is given as a superposition of a mean (time independent) solution and a sum of time-dependent wave harmonics. For the dispersive case, the dispersion coefficient is developed in terms of the horizontal wave number and amplitude of the pressure forcing at the upper surface and the vertical structure and dispersivity of the medium. The models are used to examine how dispersivity and wave parameters can influence the profiles of CO_2 within the layered medium. The impact of the location of the CO_2 source term (whether in the upper or lower layer) is also examined. Enhancement factors are developed for both the dispersive and nondispersive models in terms of permeability of the medium, the size and cross-section shape of the pore spaces, vertical structure of the medium, and the surface amplitude of the pressure forcing.

[8] In this first part of the study, the new model is shown to reinforce and extend the results of many earlier studies, which are detailed in the previous paragraphs. In part 2, *Massman and Frank* [2006] use this analytical model to estimate the time lag between the surface pressure forcing and the CO_2 response for the case of a deep snowpack overlying a layer of soil in an effort to assess whether observed undersnow CO_2 fluctuations result from, or are at least consistent with, possible advective flows induced by natural pressure pumping. They also use the model to infer information about the dispersivity of snow and the spatial and temporal characteristics of the pressure forcing.

2. Atmospheric Forcing: The Pressure Field

[9] Equations (1) and (2) are frequently used to describe atmospheric pressure pumping for a homogeneous medium [*Clarke and Waddington*, 1991; *Massmann and Farrier*, 1992; *Waddington et al.*, 1996; *Massman et al.*, 1997].

$$\frac{\partial p}{\partial t} = \kappa_p \nabla^2 p, \tag{1}$$

where p (Pa) is the fluctuating pressure field or the driving variable responsible for pressure pumping, t is time, ∇ is the gradient operator, ∇^2 is the Laplacian operator, and the pressure diffusivity, κ_p ($m^2\ s^{-1}$), is given as follows:

$$\kappa_p = \frac{P_0 k}{\eta \mu}, \tag{2}$$

where P_0 (Pa) is the mean ambient or background pressure, k (m^2) is the air permeability of the medium, η is the air-filled porosity of the medium, and μ (Pa s) is the dynamic viscosity of air. For the present purposes, variations in temperature within the porous media are not considered so that μ is uniform throughout the medium. Together, these two equations describe the "diffusion" of pressure waves through a permeable medium and follow from Darcy's law, the equation of mass conservation for air, the assumptions that $p \ll P_0$ and that the temperature of the medium is uniform in time and space [e.g., *Massman et al.*, 1997], and the compressibility of air. Other models based on the incompressibility of air have also been used to describe the fluctuating pressure field within a permeable medium [*Albert and McGilvary*, 1992], but such models are not considered in the present study because it is not clear that they are amenable to analytical solutions.

[10] Assuming p is described by a traveling or plane wave yields (in complex notation)

$$p(x,y,z,t) = A_p(z)e^{i(\omega t - \mathbf{k_h}\cdot\mathbf{r_h})}, \tag{3}$$

where x, y, and z are the spatial (Cartesian) coordinates with z being positive downward from the surface; $A_p(z)$ is the amplitude of the pressure wave as a function of depth, z; $i = \sqrt{-1}$; ω is the wave frequency, which by convention will be taken as positive ($\omega > 0$); $\mathbf{k_h} = \hat{\boldsymbol{\imath}}k_x + \hat{\boldsymbol{\jmath}}k_y$ is the horizontal wave number vector with $\hat{\boldsymbol{\imath}}$ as the unit vector in the x direction, $\hat{\boldsymbol{\jmath}}$ as the unit vector in the y direction, and k_x and k_y are the respective horizontal wave numbers; $\mathbf{r_h} = \hat{\boldsymbol{\imath}}x + \hat{\boldsymbol{\jmath}}y$; and the bold dot is the dot product of two vectors.

[11] The modeled pressure (pumping) field results from solving equations (1)–(3) for $A_p(z)$. The analytical solution for an isothermal porous medium with homogeneous physical properties [*Clarke and Waddington*, 1991; *Waddington et al.*, 1996] is

$$A_p(z) = A_p^+ e^{\beta z} + A_p^- e^{-\beta z}, \tag{4}$$

where A_p^+ and A_p^- are the complex amplitudes of the downward ($e^{\beta z}$) and upward ($e^{-\beta z}$) propagating pressure waves and

$$\beta = \sqrt{k_h^2 + i\frac{\omega}{\kappa_p}}, \tag{5}$$

where $k_h^2 = \mathbf{k_h}\cdot\mathbf{k_h} = k_x^2 + k_y^2$. Note here that β can also be written as

$$\beta = \sqrt{k_h^2 + i\frac{2}{H_p^2}}, \tag{6}$$

where $H_p = \sqrt{2\kappa_p/\omega}$ is the attenuation depth of the pressure wave.

[12] The parameter β is fundamental to characterizing different types of natural pressure pumping [*Waddington et al.*, 1996]. For example, in the case of barometric pumping (the term used to describe natural pressure pumping associated with very low frequency atmospheric pressure waves, i.e., $\omega \le 10^{-4}$ Hz), it is reasonable to assume that the horizontal wavelength of the pressure wave is much greater than H_p (i.e., $k_h \ll 1/H_p$) and therefore that $\beta \approx (i+1)/H_p$. Whereas, for static pressure pumping forced by "wavy" topography $\omega = 0$ and $\beta = k_h$.

[13] The present study assumes a two-layered medium where each layer has different, but homogeneous, properties. Therefore equation (4) is applied to each layer, and continuity of pressure or $A_p(z)$ and the vertical mass flux (proportional to $k\frac{dA_p(z)}{dz}$) are assumed across the interface between them. The upper boundary condition is the amplitude of the pressure forcing, $A_p(0)$, at the upper surface or $z = 0$. The lower boundary condition assumes an impermeable layer beneath the second model layer, which is equivalent to assuming $dA_p/dz = 0$ at the bottom of the lower layer. The model for the pressure wave is completed by solving for the two complex amplitudes A_p^+ and A_p^- for each of the two layers using these boundary and interface conditions. This method of solution has analogs in heat transfer and electromagnetic wave propagation through nonuniform media [*Karam*, 2000]. The final solutions for $A_p(z)$ and $kdA_p(z)/dz$ for either layer have the form

$$A_p(z) = F(z)A_p(0) \tag{7}$$

$$k\frac{dA_p(z)}{dz} = -k\beta G(z)A_p(0), \tag{8}$$

where for the upper layer ($0 \le z \le D_w$),

$$F_w(z) = \frac{k_w\beta_w\cosh(\beta_l D_l)\cosh[\beta_w(D_w - z)] + k_l\beta_l\sinh(\beta_l D_l)\sinh[\beta_w(D_w - z)]}{k_{wl}}$$

$$G_w(z) = \frac{k_w\beta_w\cosh(\beta_l D_l)\sinh[\beta_w(D_w - z)] + k_l\beta_l\sinh(\beta_l D_l)\cosh[\beta_w(D_w - z)]}{k_{wl}},$$

and for the lower layer ($D_w < z \le D_s$),

$$F_l(z) = \frac{k_w\beta_w\cosh[\beta_l(D_s - z)]}{k_{wl}}$$

$$G_l(z) = \frac{k_w\beta_w\sinh[\beta_l(D_s - z)]}{k_{wl}},$$

with the subscripts w and l denoting the upper or lower layers. Here D_w is the thickness of the upper layer, D_l is the thickness of the lower layer, $D_s = D_w + D_l$ is the total depth

of the permeable substrate, and $k_{wl} = k_w\beta_w \cosh(\beta_l D_l) \cosh(\beta_w D_w) + k_l\beta_l \sinh(\beta_l D_l) \sinh(\beta_w D_w)$.

3. Pressure-Induced Velocity Field

[14] Darcy's law, given next, determines the volume flux or velocity of air, **v**, forced by the pressure gradient. For the upper layer,

$$\mathbf{v_w} = -\frac{k_w}{\mu}\nabla p = -\frac{k_w}{\mu}A_p(0)\left[-i\hat{\mathbf{k_h}}k_h F_w(z) - \hat{\mathbf{k}}\beta_w G_w(z)\right]e^{i(\omega t - \mathbf{k_h}\cdot\mathbf{r_h})}. \quad (9)$$

where $\hat{\mathbf{k}}$ is the unit vector in the z-direction, $\hat{\mathbf{k_h}}$ is the unit vector in the $\mathbf{k_h}$ direction ($\hat{\mathbf{k_h}} = \mathbf{k_h}/k_h$). For the lower layer,

$$v_l = -\frac{k_l}{\mu}A_p(0)\left[-i\hat{\mathbf{k}}_\mathbf{h}k_h F_l(z) - \hat{\mathbf{k}}\beta_l G_l(z)\right]e^{i(\omega t - \mathbf{k_h}\cdot\mathbf{r_h})}. \quad (10)$$

[15] A careful examination of equations (9) and (10) shows that the horizontal component of the volume flux is not continuous across the interface between the two layers. Continuity in the vertical volume flux has been explicitly incorporated (i.e., $k_w\beta_w G_w(D_w) = k_l\beta_l G_l(D_w)$), as previously discussed, and the pressure field is continuous because $F_w(D_w) = F_l(D_w)$. However, continuity in the horizontal volume flux requires $k_w k_h F_w(D_w) = k_l k_h F_l(D_w)$ (or more precisely that $k_w k_h = k_l k_h$), which cannot be satisfied if the horizontal wavelength is the same for both layers and the permeabilities are not ($k_w \neq k_l$). Consequently, this model imposes a "slip"-like condition on the horizontal Darcian velocity at the interface between two layers with very different permeabilities. However, this discontinuity is not particularly significant to the modeling of the vertical profiles of mass or mass fluxes.

4. Advective-Diffusive Model for CO_2

[16] Assuming the trace gas (CO_2) is dilute compared to the carrier gas (air), the advective-diffusive equation for CO_2 mol fraction, χ, within the soil or snowpack is given as [e.g., *Massman et al.*, 1997]

$$\eta\frac{\partial\chi}{\partial t} + \mathbf{v}\cdot\nabla\chi - D_e\nabla^2\chi = S_\chi, \quad (11)$$

where (1) $D_e = \eta\tau D$ is the effective diffusivity ($m^2\ s^{-1}$) with D ($m^2\ s^{-1}$) denoting the diffusivity of the CO_2 in air for the ambient temperature and pressure and τ denoting the tortuosity factor of the medium ($0 < \tau \leq 1$) and (2) $S_\chi = S_{CO_2}/c$ with S_{CO_2} denoting the source term for CO_2 (mol $m^{-3}\ s^{-1}$) and c (mol m^{-3}) is the molar density of the air at ambient environmental conditions. Although no notational distinction between the upper and lower layers is made here, η, τ, D_e, and S_{CO_2} can be different for each layer.

[17] Even though the advective term $\mathbf{v}\cdot\nabla\chi$ is nonlinear, equation (11) is still amenable to an analytical solution using separation of variables and Fourier expansion. The first step is to assume the following form for the solution:

$$\chi(x,y,z,t) = \chi_0(z) + \sum_{n=1}^{\infty}\chi_n(z)e^{ni(\omega t - \mathbf{k_h}\cdot\mathbf{r_h})}, \quad (12)$$

where $\chi_0(z)$ represents the average or background CO_2 mol fraction, which is assumed to be constant in time and a function of depth only, and $\chi_n(z)$ is amplitude of nth harmonic of the time-dependent CO_2 response to the pressure forcing. Physical constraints imposed on $\chi_0(z)$ and $\chi_n(z)$ by the natural environment lead to the expectation that $\chi_n(z) \ll \chi_0(z)$. Consequently, equation (12) is a perturbation-type solution to the advective-diffusive transport equation undergoing oscillatory forcing.

[18] The second step is to derive a set of recursive inhomogeneous differential equations for each of the χ_n by equating coefficients associated with each plane harmonic wave $e^{ni(\omega t - \mathbf{k_h}\cdot\mathbf{r_h})}$. Thus the complete analytical solution is an infinite series of (harmonic) plane waves with amplitudes that are attenuated in the z direction. Combining equations (11) and (12) yields the following differential equations for χ_n. For $n = 0$,

$$-D_e\frac{d^2\chi_0}{dz^2} = S_\chi, \quad (13)$$

and for $n \geq 1$ the result is the following inhomogeneous Helmholtz equation:

$$\frac{d^2\chi_n}{dz^2} - \left(k_h^2 n^2 + \frac{i\omega\eta}{D_e}n\right)\chi_n = \frac{kA_p(0)}{\mu D_e}\cdot\left[\beta G(z)\frac{d\chi_{n-1}}{dz} + k_h^2(n-1)F(z)\chi_{n-1}\right]. \quad (14)$$

[19] The solutions to these equations are determined by the source term, S_χ and the boundary conditions. Here we assume the simplest possible model for the source term, i.e., that S_χ is uniform throughout the source layer and constant with time. For the present study, which is primarily focused on a deep snowpack overlaying a soil layer, this assumption is realistic. In this case, for the site and time period under investigation, the soil layer was nearly isothermal and dry and was, in general, a weak source of CO_2 [*Sommerfeld et al.*, 1996]. The snow layer, on the other hand, was at best a negligible source of CO_2 and, as discussed in part 2 of this study, had a relatively constant depth.

[20] The upper boundary condition on equation (13) is $\chi_0(0) = \overline{\chi}(0)$, which is taken to be a measured quantity. The lower boundary condition follows from the assumption that there is no flux into the underlying bedrock from the layer above, or $\frac{d\chi_0}{dz}(D_s) = 0$. The final boundary condition is specified at the interface and is $\chi_0(D_w) = \overline{\chi}(D_w)$, which again is taken to be a measured quantity. This last boundary condition allows S_χ to be expressed as an analytical function of the layer thicknesses and the measured mol fractions. The solution to equation (13) and S_χ is

$$\chi_0(z) = \begin{cases} \overline{\chi}(0) + \frac{\overline{\chi}(D_w) - \overline{\chi}(0)}{D_w}z & \text{for } 0 \leq z \leq D_w \\ \phi_{wl}\overline{\chi}(0) + [1-\phi_{wl}]\overline{\chi}(D_w) + \phi_{wl}\left[\frac{\overline{\chi}(D_w) - \overline{\chi}(0)}{D_w}\right]\left[z - \frac{(z-D_w)^2}{2D_l}\right] & \text{for } D_w \leq z \leq D_s. \end{cases} \quad (15)$$

$$S_\chi = D_e^w\frac{\overline{\chi}(D_w) - \overline{\chi}(0)}{D_w D_l}, \quad (16)$$

where $\phi_{wl} = \eta_w\tau_w/(\eta_l\tau_l)$ and $D_e^w = \eta_w\tau_w D$.

[21] The solution to the homogeneous part of equation (14), i.e., the complementary solution, $\chi_n^c(z)$, for the no-source upper layer is

$$\chi_n^c(z) = A_{\chi_n}^+ e^{\lambda_{wn} z} + A_{\chi_n}^- e^{-\lambda_{wn} z}, \tag{17}$$

where $\lambda_{wn} = \sqrt{k_h^2 n^2 + \frac{i\omega\eta_w}{D_e^w} n}$ and $A_{\chi_n}^+$ and $A_{\chi_n}^-$ are the complex amplitudes of the nth harmonic downward ($e^{\lambda_{wn} z}$) and upward ($e^{-\lambda_{wn} z}$) "waves" of CO_2 mol fraction.

[22] The solution to the inhomogeneous part of equation (14), i.e., the particular solution, $\chi_n^p(z)$, depends on n. The $n = 1$ solution for the no-source upper layer is

$$\chi_1^p(z) = \left[\frac{k_w A_p(0)}{\mu D_e^w}\right]\left[\frac{\overline{\chi}(D_w) - \overline{\chi}(0)}{D_w}\right]\left[\frac{\beta_w}{\beta_w^2 - \lambda_{w1}^2}\right] G_w(z). \tag{18}$$

Note here that it is possible to continue the solution series for $n \geq 2$. However, this is not necessary for the present study because, as discussed in part 2, there is little observational evidence to support the inclusion of any higher harmonics.

[23] The boundary conditions for the mass transfer model, equation (14), are similar to, but not exactly the same as, those outlined for the model of the pressure field (i.e., equation (4)). As in the pressure model, an amplitude at the upper boundary is specified. It will be denoted as $A_{\chi_1}(0)$. The lower boundary condition is also a no-flux condition, and at the interface between the two layers the solutions and the corresponding fluxes are matched as with the pressure field.

[24] With these boundary conditions and matching constraints, the solution to equation (14) for the snowpack ($0 \leq z \leq D_w$) is

$$\chi_1(z) = h_4 \sinh(\lambda_{w1} z) + \left\{A_{\chi_1}(0) - \gamma_{w\chi_1} G_w(0)\right\} e^{-\lambda_{w1} z} + \gamma_{w\chi_1} G_w(z), \tag{19}$$

and for the soil ($D_w \leq z \leq D_s$) it is

$$\chi_1(z) = h_3 \cosh[\lambda_{l1}(D_s - z)] + \gamma_{l\chi_1}\left(\frac{D_s - z}{D_l}\right)\sinh[\beta_l(D_s - z)] + \gamma_{l\chi_1}^c \cosh[\beta_l(D_s - z)], \tag{20}$$

where

$$h_4 = \frac{h_3 \cosh(\lambda_{l1} D_l) + h_1}{\sinh(\lambda_{w1} D_w)},$$

$$h_3 = \frac{h_2 \sinh(\lambda_{w1} D_w) - h_1 \sinh(\lambda_{w1} D_w)}{\cosh(\lambda_{l1} D_l)\cosh(\lambda_{w1} D_w) + \frac{\lambda_{l1}}{\phi_{wl}\lambda_{1w}}\sinh(\lambda_{l1} D_l)\sinh(\lambda_{w1} D_w)},$$

$$h_2 = \frac{-\gamma_{l\chi_1}\sinh(\beta_l D_l)/D_l - \gamma_{l\chi_1}\beta_l\cosh(\beta_l D_l) - \gamma_{\chi_1}^c\beta_l\sinh(\beta_l D_l) + \phi_{wl}\gamma_{w\chi_1}\beta_w F_w(D_w)}{\phi_{wl}\lambda_{w1}} + \left\{A_{\chi_1}(0) - \gamma_{w\chi_1} G_w(0)\right\} e^{-\lambda_{w1} D_w},$$

$$h_1 = \gamma_{l\chi_1}\sinh(\beta_l D_l) + \gamma_{l\chi_1}^c \cosh(\beta_l D_l) - \left\{A_{\chi_1}(0) - \gamma_{w\chi_1} G_w(0)\right\} e^{-\lambda_{w1} D_w} - \gamma_{w\chi_1} G_w(D_w),$$

with

$$\gamma_{w\chi_1} = \left[\frac{k_w A_p(0)}{\mu D_e^w}\right]\left[\frac{\overline{\chi}(D_w) - \overline{\chi}(0)}{D_w}\right]\left[\frac{\beta_w}{\beta_w^2 - \lambda_{w1}^2}\right]$$

$$\gamma_{l\chi_1} = \left[\frac{k_w A_p(0)}{\mu D_e^l}\right]\left[\frac{\overline{\chi}(D_w) - \overline{\chi}(0)}{D_w}\right]\left[\frac{\beta_w k_l \beta_l}{(\beta_l^2 - \lambda_{l1}^2) k_{lw}}\right],$$

(where λ_{l1} is the soil analog to λ_{w1}) and

$$\gamma_{l\chi_1}^c = -\left[\frac{2\beta_l/D_l}{\beta_l^2 - \lambda_{l1}^2}\right]\gamma_{l\chi_1}.$$

[25] However, there is a fifth boundary condition imposed on equations (19) and (20) at the snowpack/soil interface ($z = D_w$). The magnitude of the complex solution at this interface, $|\chi_1(D_w)|$, is to be specified and henceforth is denoted by $A_{\chi_1}(D_w)$. This last boundary condition is important because, as discussed in part 2, it can be measured (at least for very low frequencies). However, $A_{\chi_1}(D_w)$ must be imposed on $\chi_1(z)$ at $z = D_w$ in such a way as to keep the phase of the solution consistent across the interface. This is accomplished using an iterative numerical method described in Appendix A. (Note that all model profiles are displayed graphically in section 6.)

[26] Before ending this section, there are two points concerning the mass flow model that need some discussion. First, the model is expressed in terms of an amplitude, $A_{\chi_1}(0)$, as an upper boundary condition. Generally speaking this amplitude may not be measurable in a natural setting, so it is important to be able to estimate or parameterize it in terms of the pressure forcing and the physical constraints imposed on it by the medium itself. Such a parameterization is developed in section 7, which discusses the diffusive flux enhancement factors. Second, if $\beta_w = \lambda_{w1}$, equation (18) would become undefined, indicating that the mass flow model is potentially subject to resonance. This is true for either model layer regardless of the relative positioning of the source term. From the general definitions of β and λ_1, resonance will occur in the mass flow model whenever $\frac{k}{\eta\tau} = \frac{\mu D}{P_0}$. For most conditions encountered at the Earth's surface, $\mu D/P_0 = (2\text{—}8) \times 10^{-15}$ m^2, well below $k/(\eta\tau)$ values for most soils and snowpacks [e.g., *Albert et al.*, 2000; *Massman et al.*, 1997; *Freeze and Cherry*, 1979].

5. Dispersive-Diffusive Model for CO_2

[27] In soils (as well as snowpacks), dispersion results from mechanical mixing caused by the interaction between the flow and the structural inhomogeneities of the medium. It is typically parameterized in terms of the advective velocity and a length scale (or dispersivity (m)) that is characteristic of the medium [*Bear*, 1972; *Labolle and Fogg*, 2001; *Lichtner et al.*, 2002] and the physical dimensions of the volume of the medium undergoing advective flows [*Perfect*, 2003]. Generalizing equation (11) to include the effects of dispersivity of the permeable medium yields

$$\eta\frac{\partial\chi}{\partial t} + \mathbf{v}\cdot\boldsymbol{\nabla}\chi - D_e\nabla^2\chi - \boldsymbol{\nabla}\cdot\underline{\boldsymbol{\mathcal{D}}}\cdot\boldsymbol{\nabla}\chi = S_\chi, \tag{21}$$

where $\underline{\boldsymbol{\mathcal{D}}}$ (m^2 s^{-1}) is the dispersion tensor, and the dispersive term that is proportional to $\nabla c/c$, which is relatively small, has been neglected. To extend the previous (nondispersive) analytical model to include dispersion, some simplification of the dispersivity tensor is necessary.

[28] For an isotropic medium, $\underline{\boldsymbol{\mathcal{D}}}$ can be expressed as follows:

$$\underline{\mathcal{D}} = \begin{pmatrix} \alpha_T v + (\alpha_L - \alpha_T)\frac{v_x v_x}{v} & (\alpha_L - \alpha_T)\frac{v_x v_y}{v} & (\alpha_L - \alpha_T)\frac{v_x v_z}{v} \\ (\alpha_L - \alpha_T)\frac{v_y v_x}{v} & \alpha_T v + (\alpha_L - \alpha_T)\frac{v_y v_y}{v} & (\alpha_L - \alpha_T)\frac{v_y v_z}{v} \\ (\alpha_L - \alpha_T)\frac{v_z v_x}{v} & (\alpha_L - \alpha_T)\frac{v_z v_y}{v} & \alpha_T v + (\alpha_L - \alpha_T)\frac{v_z v_z}{v} \end{pmatrix},$$

where α_T is the transverse dispersivity (m), α_L is the longitudinal dispersivity (m), $\mathbf{v_x}$, $\mathbf{v_y}$, and $\mathbf{v_z}$ are the velocity components, and $v = \sqrt{v_x^2 + v_y^2 + v_z^2}$ is the magnitude of the vector velocity. To keep this model analytically tractable, $\alpha_L = \alpha_T = \alpha$ is assumed. In general, this is not the case because α_L is usually an order of magnitude greater than α_T [*Gelhar et al.*, 1992]. However, *Labolle and Fogg* [2001] found with their modeling effort that solute migration is largely insensitive to α_L (at least for molecular or microscale flows, which can be characterized as $\alpha_T \approx 0.01$ m). Nevertheless, regardless of whether the flows are microscale or macroscale, the main impact of assuming $\alpha_L = \alpha_T$ on the present model is that (1) the total dispersion coefficient corresponding to the diagonal terms of the dispersivity matrix are underestimated by a small amount and (2) the dispersion associated with the off-diagonal elements can be ignored. This simplification diagonalizes the dispersion tensor, reducing it to the unity tensor times a scalar, $\mathcal{D}(z)$, which is

$$\mathcal{D}(z) = \alpha\left[\frac{kA_p(0)}{\mu}\right]\mathrm{Sgn}\left(\Re\left\{\left[\sqrt{k_h^2 F(z)^2 + \beta^2 G(z)^2}\right] e^{i(\omega t - \mathbf{k_h}\cdot\mathbf{r_h})}\right\}\right) \cdot \left[\sqrt{k_h^2 F(z)^2 + \beta^2 G(z)^2}\right] e^{i(\omega t - \mathbf{k_h}\cdot\mathbf{r_h})},$$

where Sgn is the Signum function: Sgn(x) = sign of x and $\Re\{\}$ indicates the real part. The above expression for $\mathcal{D}(z)$ results from the velocity equations (9) and (10) and the Signum function is associated with v, the magnitude of the velocity [*Lichtner et al.*, 2002], which insures that dispersion enhances (rather than reverses) diffusion. $\mathcal{D}(z)$ can be further simplified to

$$\mathcal{D}(z) = \alpha\left[\frac{kA_p(0)}{\mu}\right]\left[\sqrt{k_h^2|F(z)|^2 + |\beta G(z)|^2}\right]\mathrm{Sgn} \cdot \left(\Re\left\{e^{i(\omega t - \mathbf{k_h}\cdot\mathbf{r_h})}\right\}\right) e^{i(\omega t - \mathbf{k_h}\cdot\mathbf{r_h})}, \quad (22)$$

where $|x|$ indicates the absolute value of x. This simplification to $\sqrt{k_h^2 F(z)^2 + \beta^2 G(z)^2}$ is extremely good when the permeabilities of the upper and lower model layers are the same. For the case of differing permeabilities the results are still quite good for the upper layer, but it does misrepresent the magnitude of the advective velocity for the lower layer. However, advective velocities are so low in the lower layer that this inaccuracy should have very little impact on any modeling results. Equation (21) is thus simplified to

$$\eta\frac{\partial\chi}{\partial t} + \mathbf{v}\cdot\boldsymbol{\nabla}\chi - D_e\nabla^2\chi - \mathcal{D}(z)\nabla^2\chi - [\nabla\mathcal{D}(z)]\cdot[\boldsymbol{\nabla}\chi] = S_\chi. \quad (23)$$

[29] Next, because both χ and $\mathcal{D}$ have the same wave formulation in the horizontal, it is useful to note the equivalency: $\mathcal{D}(z)\nabla_h^2\chi = \boldsymbol{\nabla}_h\mathcal{D}(z)\cdot\boldsymbol{\nabla}_h\chi$, where the h subscript refers to the horizontal portions of the gradient and Laplacian operators. In addition to this equivalency, two other simplifications are necessary: one involving $\mathcal{D}(z)$, the other involving $\partial\mathcal{D}(z)/\partial z$. Numerical test and comparisons suggested that: $\sqrt{k_h^2|F(z)|^2 + |\beta G(z)|^2} \approx \sqrt{k_h^2 + |\beta G(0)|^2}$ for $\mathcal{D}(z)$ and $\partial\mathcal{D}(z)/\partial z \approx -|\beta G(0)|\mathcal{D}(z)$. Including the equivalency and the two simplifications yields

$$\eta\frac{\partial\chi}{\partial t} + \mathbf{v}\cdot\boldsymbol{\nabla}\chi - D_e\nabla^2\chi - 2\mathcal{D}\nabla_\mathbf{h}^2\chi - \mathcal{D}\frac{\partial^2\chi}{\partial z^2} + \mathcal{D}|\beta G(0)|\frac{\partial\chi}{\partial z} = S_\chi, \quad (24)$$

where $\mathcal{D} = \left[\frac{kA_p(0)}{\mu}\right]\left[\alpha\sqrt{k_h^2 + |\beta G(0)|^2}\right]\mathrm{Sgn}(\Re\{e^{i(\omega t - \mathbf{k_h}\cdot\mathbf{r_h})}\})$ $e^{i(\omega t - \mathbf{k_h}\cdot\mathbf{r_h})}$ is constant within a given layer of the model.

[30] Of these latter two approximations, the first is quite good. However, the second, being one of several approximations that could have been used, is relatively conservative. In general, this second approximation is more dependent on ω and k_h than the first approximation, and it improves at the higher frequencies and higher wave numbers relative to the lower frequencies and longer wavelengths. Nevertheless, at most frequencies this velocity shear related term, $\mathcal{D}|\beta G(0)|\partial\chi/\partial z$, is negligible compared to the dispersive-diffusive term, $-\mathcal{D}\partial^2\chi/\partial z^2$. However, the shear-related term does increase with increasing ω and k_h, so that it can become significant at high enough frequencies or short enough horizontal wavelengths. As discussed later, this suggests that the present formulation of the shear-related term may exclude the dispersive model for use in describing very high frequency forcing.

[31] It is possible to use the same perturbation approach to derive an analytical solution to equation (24) as that used for deriving the analytical model of equation (11). However, first it is necessary to approximate the wave part, [Sgn ($\Re\{e^{i(\omega t - \mathbf{k_h}\cdot\mathbf{r_h})}\}$) $e^{i(\omega t - \mathbf{k_h}\cdot\mathbf{r_h})}$], of $\mathcal{D}$ (equation (22)) for both the mean field and perturbation equations. This can be done using the first term of the Fourier series appropriate to either χ_0 or χ_1. These approximations are based upon the following Fourier expansions: Sgn[cos(x)] cos(x) = |cos(x)| = $2/\pi + 4\cos(2x)/(3\pi) + \cdots$ for χ_0 and |cos(x)|cos(x) = $8\cos(x)/(3\pi) + 8\cos(3x)/(15\pi) + \cdots$ for χ_1. The simplification is achieved because only the first terms of each expansion are kept. Incorporating higher harmonics is not necessary since only χ_0 and χ_1 are sufficient for the present purposes (as discussed in part 2). This is equivalent to making the following assignments for $\mathcal{D}$: $\mathcal{D} = [\frac{2}{\pi}][\alpha\sqrt{k_h^2 + |\beta G(0)|^2}][\frac{kA_p(0)}{\mu}]$ for the mean field equation and $\mathcal{D} = [\frac{8}{3\pi}][\alpha\sqrt{k_h^2 + |\beta G(0)|^2}][\frac{kA_p(0)}{\mu}]$ in the equation describing $\chi_1(z)$. However, given the uncertainty in any estimate of dispersivity and that $8/(3\pi) \approx 1$, the $8/(3\pi)$ factor will be subsumed into α, but the ratio between the expressions for $\mathcal{D}$ in the mean and perturbation equations will be preserved. The resulting and final models for the

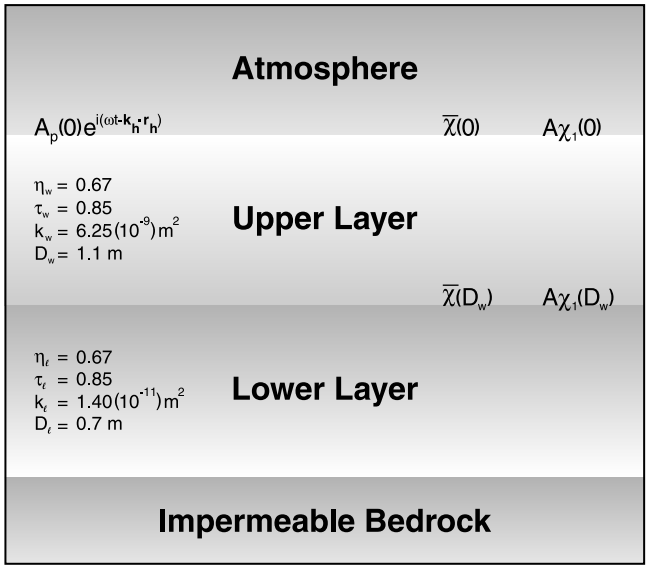

Figure 1. Schematic of model domain with snowpack and soil parameter values and key model variables. The model parameters are taken largely from *Massman et al.* [1997].

mean (steady state) and (n = 1) perturbation portions of the dispersive flow model are

$$-\left(D_e+\frac{3}{4}\mathcal{D}\right)\frac{d^2\chi_0}{dz^2}+\left[\frac{3}{4}\mathcal{D}|\beta G(0)|\right]\frac{d\chi_0}{dz}=S_\chi \qquad (25)$$

$$\frac{d^2\chi_1}{dz^2}-\left(\frac{\mathcal{D}|\beta G(0)|}{D_e+\mathcal{D}}\right)\frac{d\chi_1}{dz}-\left(\frac{D_e+2\mathcal{D}}{D_e+\mathcal{D}}k_h^2+\frac{i\omega\eta}{D_e+\mathcal{D}}\right)\cdot\chi_1=\frac{kA_p(0)}{\mu(D_e+\mathcal{D})}\left[\beta G(z)\frac{d\chi_0}{dz}\right], \qquad (26)$$

where $\mathcal{D}$ is now given as $[\alpha\sqrt{k_h^2+|\beta G(0)|^2}]\ [kA_p(0)/\mu]$. Note that the equations describing the nondispersive pressure pumping model are recovered if $\mathcal{D}$ = 0, so that these last two equations generalize the original model.

[32] The method of solving these coupled equations proceeds as before. All boundary conditions and interface matching conditions are the same, except that the definition of flux has changed slightly. The flux associated with the steady state solution is now defined as $-[D_e + 3\mathcal{D}/4]d\chi_0/dz + [3\mathcal{D}|\beta G(0)|/4]\chi_0$. The perturbation field has a similar definition for the instantaneous flux: $-[D_e + \mathcal{D}]d\chi_1/dz + [\mathcal{D}|\beta G(0)|]\chi_1$. The analytical solutions to these equations are presented graphically in the next section.

6. Modeled CO_2 Profiles

[33] Figure 1 gives a schematic overview of the model, its domain and structure, and the important input variables along with their numerical values. Figure 2 shows four examples of the model profiles for the steady state solution, $\chi_0(z)$. These profiles correspond to nondispersive and highly dispersive substrates for the cases where the source term is located in either the upper or lower layer. Note that although this study is focused primarily on the case where S_χ is in the lower layer with a passive upper layer, the reverse

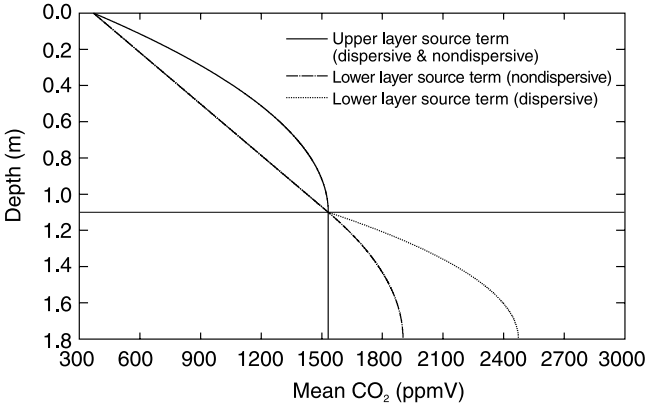

Figure 2. Steady state CO_2 model profiles, $\chi_0(z)$. In the case of the CO_2 source term located in the upper layer, only one curve is shown for the dispersive and nondispersive substrates because the two corresponding curves are virtually indistinguishable. The thin horizontal line at a depth of 1.1 m represents the interface between the upper and lower layers.

case is included here for the purposes of exploring model sensitivity. Except for α, $A_p(0)$, $A_{\chi_1}(0)$, and sometimes $A_{\chi_1}(D_w)$ (all discussed below), all the specific values chosen for the boundary conditions and the physical parameters that define the two permeable layers are taken from observations and discussed in more detail in part 2. In this first part of this study the pertinent values of these model input parameters are stated without elaboration. For these simulations, $\overline{\chi}(0)$ = 375 ppm and $\overline{\chi}(D_w)$ = 1532 ppm. For the dispersive cases, $D_e = 1.13 \times 10^{-5}\ m^2\ s^{-1}$, $\mathcal{D}_w = 2.33 \times 10^{-5}\ m^2\ s^{-1}$, and $\mathcal{D}_l = 5.29 \times 10^{-7}\ m^2\ s^{-1}$. In this and the next two figures, wherever the solid and dashed lines overlap the dispersive and nondispersive cases are nearly identical.

[34] Figure 3 shows the profiles of the low-frequency perturbation field, $\chi_1(z)$, for the same choice of parameter values as Figure 1. For this simulation, $\omega = 1.0 \times 10^{-5}\ s^{-1}$, corresponding to a wave period of about 7.25 days. The

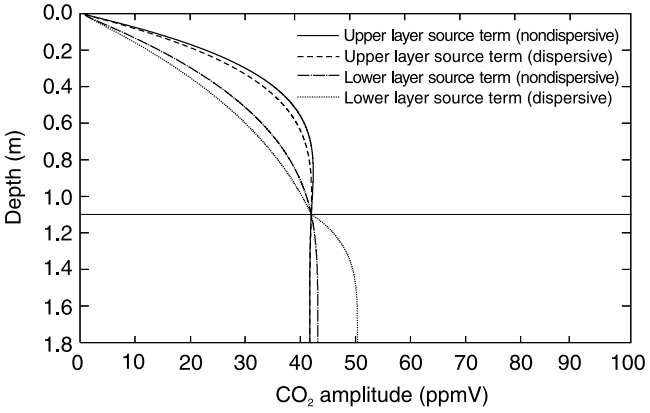

Figure 3. Model perturbation CO_2 profiles, $\chi_1(z)$, corresponding to very low frequency forcing. Where the solid and dashed lines overlap, only the solid line is shown. The thin horizontal line at a depth of 1.1 m represents the interface between the upper and lower layers.

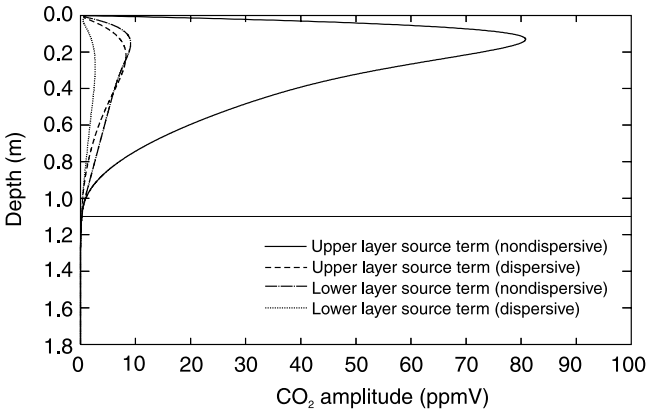

Figure 4. Model perturbation CO_2 profiles, $\chi_1(z)$, corresponding to high-frequency forcing. The thin horizontal line at a depth of 1.1 m represents the interface between the upper and lower layers.

associated wavelength is assumed to be 10^5 m. $A_{\chi_1}(0)$ = 1.0 ppm is chosen arbitrarily and mostly for convenience; but, $A_{\chi_1}(D_w)$ = 42 ppm was taken from observed under-snow data. The forcing amplitude $A_p(0)$ = 10 Pa, is fixed for all simulations. However, 10 Pa is likely to underestimate the true amplitude of the pressure forcing on such low-frequency synoptic scales where 100 Pa $\leq A_p(0) \leq$ 1000 Pa is more typical. However, for these simulations the major driving variable for dispersive flows is the product $\alpha A_p(0)$. Consequently, α is adjusted to compensate for the fixed value of $A_p(0)$ such that $\mathcal{D}_w \approx 2D_e^w$ for highly dispersive flows. For this simulation the dispersivity, α = 100 m.

[35] Figure 4 shows the profiles of the high-frequency perturbation field, $\chi_1(z)$, for the same choice of parameter values as Figure 1. For this simulation, $\omega = 5.2 \times 10^{-3}$ s^{-1}, corresponding to a wave period of about 20 min and a wavelength of 10 m. This figure is intended to suggest how atmospheric turbulence might influence the substrate CO_2 profiles. As before $A_{\chi_1}(0)$ = 1.0 ppm; but now, $A_{\chi_1}(D_w)$ = 0.25 ppm is chosen arbitrarily. For this simulation α = 0.01 m, $\mathcal{D}_w = 2.72 \times 10^{-5}$ m^2 s^{-1}, and $\mathcal{D}_l = 6.09 \times 10^{-7}$ m^2 s^{-1}.

[36] Figure 2 suggests that the importance of dispersivity to the mean profiles (at least for the present examples) is primarily confined to the lower layer when the source term is located there. This is a consequence of the fact that dispersion should increase the fluxes emanating from the soil and from the snowpack. However, now that the flux estimate is greater with dispersion than without it, the corresponding estimates for both the source term and the amount of CO_2 stored within the source layer are also greater. However, in the present study these changes in the source strength result only from mathematical consistencies imposed by the modeling assumptions, they should not be understood as implying that any physical or "real" source term is determined by the fluxes. That said, it is important to realize that the present results clearly indicate the importance of advective flows to CO_2 profiles and fluxes within and near any source region. Consequently, any model of soil CO_2 based on simple diffusion with a source term driven by environmental and intrinsic parameters (e.g., temperature, soil moisture, microbial growth kinetics) runs the risk of significantly misrepresenting the CO_2 storage and fluxes during periods when naturally occurring pressure fluctuations induce advective flows within the soil.

[37] Figures 3 and 4 both indicate that dispersivity can influence the substrate profiles of CO_2. However, clearly the impact is greater at high frequencies than at low frequencies. At both high and low frequencies the amplitude of χ_1 within the substrate is reduced as dispersivity increases. This is consistent with the finding, discussed in more detail in section 7, that the advective flux associated with the perturbation field is less in a dispersive medium than a nondispersive medium, assuming all other things remain equal. Although less important to the present study, these last two figures also indicate that the location of the source term influences CO_2 profiles in such a way as to magnify the effects of the forcing or dispersivity.

[38] To this point of the study, the focus has been on the analytical models of the trace gas profiles within the substrate. Consequently, the pressure forcing wave and the CO_2 response wave were expressed in terms of their respective amplitudes, $A_p(0)$ and $A_{\chi_1}(0)$. The next section develops mathematical expressions for the CO_2 flux that can be used independent of the substrate CO_2 profiles and uses *Chatwin*'s [1975] model (in a manner similar to *Webster* [2003]) to derive expressions of the enhancement of simple diffusion by naturally occurring oscillatory dispersive flows in soils and snowpacks. Expanding the discussion to include model fluxes and the enhancement factor has two important benefits. First, *Chatwin*'s [1975] enhancement factor makes it possible to express the wave amplitudes (or upper and lower boundary conditions) $A_{\chi_1}(0)$ and $A_{\chi_1}(D_w)$ in terms of the forcing amplitude $A_p(0)$ (plus some structural characteristics of the permeable substrate). Therefore, as pointed out at the end of section 4, in so far as $A_{\chi_1}(0)$ may be very difficult or even impossible to measure directly, a model of the enhancement factor can provide an alternative method for estimating it. Second, highlighting the model fluxes can provide insights and guidance for subsequent modeling and observational studies of pressure pumping in soils and snowpacks.

7. Advective Fluxes and Diffusive Flux Enhancement Factors

7.1. Nondispersive Fluxes

[39] For a nondispersive medium the mean or net vertical flux emanating from a snowpack undergoing periodic pressure forcing, $\overline{F}_\chi(0)$, is composed of a mean diffusive flux, $F_{diff}(0)$, and a mean advective wave flux, $F_{wave}(0)$, as follows:

$$\overline{F}_\chi(0) = D_e^w \frac{\overline{\chi}(D_w) - \overline{\chi}(0)}{D_w} + \frac{k_w}{4|\mu} A_p(0) A_{\chi_1}(0) \Re\{\beta_w G_w(0)\}, \tag{27}$$

where the first term of on the right-hand side of equation (27) is $F_{diff}(0)$ and the second term is $F_{wave}(0)$, which is obtained as the covariance between the two sinusoidal waves $\hat{\mathbf{k}} \cdot \mathbf{v}$ and χ_1 [e.g., *Watson*, 1983].

[40] Before proceeding to the dispersive case, equation (27) can be used to examine the relative importance of different types of natural pressure forcing to flux enhance-

ment. The key parameter at this point of the discussion is $\Re\{\beta_w G_w(0)\}$.

[41] First, consider barometric pressure pumping associated with synoptic scale atmospheric motions with wave period about a week ($\omega \approx 10^{-5}$ s^{-1}), for which $\beta_w \approx (i+1)/H_{pw}$ and $G_w(0) \approx (i+1)(\frac{D_w}{H_{pw}} + \sqrt{\frac{k_l}{k_w}}\frac{D_l}{H_{pw}})$; where $H_{pw} = \sqrt{\frac{2P_0 k_w}{\eta_w \mu \omega}}$. In this case, $\beta_w G_w(0)$ is nearly purely imaginary and $\Re\{\beta_w G_w(0)\} \approx 0$, indicating, in agreement with previous studies [*Waddington et al.*, 1996], that barometric pressure pumping is unlikely to have much effect on trace gas fluxes from snowpacks.

[42] Next consider topographically induced pressure forcing ($\omega = 0$). For this case, both β_w and $G_w(0)$ are real quantities and therefore $\Re\{\beta_w G_w(0)\} = \beta_w G_w(0)$. Therefore, if all other things are held fixed, the wave flux associated with topographic pressure forcing will exceed the corresponding low-frequency $F_{wave}(0)$. In turn this suggests that topographically induced pressure forcing could significantly enhance diffusive fluxes. *Colbeck* [1989] found similar results.

[43] As the final example, consider pressure forcing driven by atmospheric turbulence (10^{-3} s$^{-1} \leq \omega \leq 10^{-1}$ s^{-1}), for which both β_w and $G_w(0)$ are complex so that $\Re\{\beta_w G_w(0)\} > 0$. This type of natural forcing therefore is intermediate between the two previous examples, indicating that atmospheric turbulence may also enhance the mean flux evolving from the snowpack. However, the relative importance of this type of forcing to the total flux will depend, in part, on the relative contributions of k_h^2 and ω/κ_p to β_w (equation (5)).

7.2. Dispersive Fluxes

[44] For a dispersive medium $F_{wave}(0)$ remains the same. However, equation (25) indicates there are two additional flux components: the gradient-dispersive flux, $F_{gd}(0) = \frac{3}{4}\mathcal{D} d\chi_0/dz$, which for the case of a snowpack overlying a soil is proportional to $\mathcal{D}_w[\overline{\chi}(D_w) - \overline{\chi}(0)]$, and the shear-dispersive flux, $F_{sd}(0) = -\frac{3}{4}\mathcal{D}|\beta G(0)|\chi_0$, which under the same snowpack/soil scenario above is proportional to $-\mathcal{D}_w|\beta_w G(0)|\overline{\chi}(0)$. However, unlike $F_{wave}(0)$, which results from the interaction of the perturbation fields $\hat{\mathbf{k}}\cdot\mathbf{v}$ and χ_1, $F_{gd}(0)$ and $F_{sd}(0)$ result from a quasi steady state advective flow ($v \propto [\mathrm{Sgn}\,(\Re\{e^{i(\omega t - \mathbf{k_h}\cdot\mathbf{r_h})}\})\, e^{i(\omega t - \mathbf{k_h}\cdot\mathbf{r_h})}]$) interacting with the mean or steady state CO_2 field.

[45] For the case of a snowpack (nonsource) overlaying the soil (source) the gradient-dispersive flux is

$$F_{gd}(0) = \frac{3}{4}\mathcal{D}_w\left[\frac{\sigma_w|\beta_w G(0)|}{e^{\sigma_w|\beta_w G(0)|D_w} - 1}\right][\overline{\chi}(D_w) - \overline{\chi}(0)], \qquad (28)$$

and the shear-dispersive flux is

$$F_{sd}(0) = -\frac{3}{4}\mathcal{D}_w|\beta_w G(0)|\overline{\chi}(0), \qquad (29)$$

where $\sigma_w = \frac{3}{4}\mathcal{D}_w/(D_e^w + \frac{3}{4}\mathcal{D}_w)$. Note here that $F_{gd}(0)$ takes on slightly different expressions depending on the location of the source term; however, $F_{sd}(0)$ is the same for either source location. Further note here that because the shear-dispersive flux is negative, it reduces the overall diffusive enhancement by opposing the gradient-dispersive flux. However, for the modeling scenarios examined in the present study, $|F_{sd}(0)| \ll F_{gd}(0)$, which indicates that the dispersive model is consistent with the expectation that dispersion augments diffusion (or more specifically dispersion enhances the coefficient of diffusion).

7.3. Enhancement Factor

[46] In general the diffusive enhancement factor, R, is the ratio of an advective flux to the diffusive flux. For $F_{gd}(0)$ and $F_{sd}(0)$, R can easily be determined from the last two equations and the definition of $F_{diff}(0)$ from equation (27). However, $R_{wave} = F_{wave}(0)/F_{diff}(0)$ is better expressed without explicitly including $A_{\chi_1}(0)$. Since the basic approach for accomplishing this is the same regardless of dispersivity of the medium, the nondispersive case is presented first.

[47] In *Chatwin*'s [1975] model, R_{wave} is proportional to the square of the pressure gradient, where the constant of proportionality ($\mathcal{F}$) is a function of the Schmidt (S_c) and Wormersley (W_o) numbers, the radius of the tube (a (m)), and the kinematic viscosity (ν (m^2 s^{-1})) [*Watson*, 1983]. Assuming that the pore system of the substrate is composed of a network of cylindrical capillary tubes each of uniform radius, which are randomly but uniformly distributed in all directions, *Webster* [2003] extended Chatwin's and Watson's results to yield

$$R_{wave} \propto \frac{\eta_w}{3}\left[\frac{\mathcal{F}(S_c, W_o, a, \nu)}{5}\Re^2\{ik_h F_w(0)\} + \frac{3\mathcal{F}(S_c, W_o, a, \nu)}{5}\Re^2 \cdot \{\beta_w G_w(0)\}\right]\frac{\nu^2}{\mu^2}A_p^2(0),$$

where $S_c = \nu/D$, and $W_o = (a^2\omega/\nu)^{1/2}$. The first term of this expression, $\eta_w/3$, is the effective diffusivity correction, which from equation (11) should be given by $\eta_w\tau_w$. For a sandy underwater sediment $\tau \approx 1/3$ may not be unreasonable [*Webster*, 2003]. However, for many soils and most snowpacks, τ often exceeds 1/3 by a factor of 2 or more [*Du Plessis and Masliyah*, 1991; *Massman et al.*, 1997]. Consequently, the randomly distributed tube model underpredicts the true tortuosity for many permeable substrates at the Earth's surface, suggesting of course that tubes of pore space in natural permeable media are probably not randomly distributed [*Saffman*, 1960]. To compensate for this underestimation, the above expression is adjusted by replacing $\eta_w/3$ by $\eta_w\tau_w$ and then dropping the factor of 3/5 that multiplies $\Re^2\{\beta_w G_w(0)\}$ (the second term enclosed in square brackets in the above proportionality). Combining these simplifications with the approximation $\Re\{ik_h F_w(0)\} = 0$, which is quite reasonable for the present study, R_{wave} can be expressed as

$$R_{wave} = \mathcal{F}(S_c, W_o, a, \nu)\Re^2\{\beta_w G_w(0)\}\frac{\nu^2}{\mu^2}A_p^2(0). \qquad (30)$$

Note here that the factor $\eta_w\tau_w$ has been subsumed into $F_{diff}(0)$ and therefore has been eliminated from equation (30).

[48] The factor $\mathcal{F}(S_c, W_o, a, \nu)$ can be obtained from *Watson* [1983] by noting first that $S_c \approx 1$ for air and CO_2, and second that for most naturally occurring atmospheric driving frequencies and permeable substrates at the Earth's surface, at a minimum, $W_o < 1$ can be expected and that $W_o \ll$

Table 1. Model Vertical Surface CO_2 Component Fluxes (ppm m s^{-1}) at Low and High Forcing Frequencies for Dispersive and Nondispersive Snowpack Overlying a Soil, Which is Assumed to Be the CO_2 Source[a]

Frequency	Nondispersive		Dispersive			
ω, s^{-1}	$F_{diff}(0)$	$F_{wave}(0)$ [M]	$F_{diff}(0)$	$F_{wave}(0)$ [M]	$F_{gd}(0)$	$F_{sd}(0)$
1.0×10^{-5}	0.12×10^{-1}	0.34×10^{-21} [1.4]	0.12×10^{-1}	0.15×10^{-22} [6.5]	0.18×10^{-1}	$-.31 \times 10^{-8}$
5.2×10^{-3}	0.12×10^{-1}	0.26×10^{-5} [1.4]	0.10×10^{-1}	0.71×10^{-7} [7.7]	0.19×10^{-1}	$-.28 \times 10^{-2}$

[a]Positive values of the fluxes indicate that they are upward from the snow surface into the atmosphere. The values for $F_{wave}(0)$ assume that the pore space tubes have a cylindrical cross section. $F_{wave}(0)$ for a pore tube with a rectangular cross section can be found by multiplying the tabulated value of $F_{wave}(0)$ by the number enclosed in square brackets, [M], to the right of these values.

1 is probable (or equivalently that $W_o \approx 0$). Under these conditions, $\mathcal{F}(S_c, W_o, a, \nu) = (S_c^4/6144)(a^6/\nu^4)$. Next, combining this expression for $\mathcal{F}$ with the relationship $a^6/k_w^3 = (24/\eta_w)^3$ valid for cylindrical tubes [*Webster*, 2003; *Saffman*, 1960] yields the following expression for the enhancement factor R_{wave}^{cyc} for a permeable medium composed of pore spaces shaped like cylindrical tubes:

$$R_{wave}^{cyc} = \left[\frac{S_c^4}{6144}\left(\frac{24}{\eta_w}\right)^3\right]\left[k_w \Re^2\{\beta_w G_w(0)\}\right]\left[\frac{A_p^2(0)k_w^2}{\mu^2\nu^2}\right], \quad (31)$$

where k_w^3 has been included such that each term enclosed in a square bracket on the right hand side of this expression is dimensionless.

[49] Even though equation (31) is valid for a permeable medium with cylindrical pore tubes, much of the logic used to derive this expression is also valid for pore space tubes with rectangular cross sections, except that the tube-shape geometry factor, $[\frac{S_c^4}{6144}(\frac{24}{\eta_w})^3]$, is different. In the case of a rectangular cross section, *Watson*'s [1983] model suggests that $\mathcal{F}(S_c, W_o, a, \nu) = (S_c^2/945)(h^6/\nu^4)$ and the model of *Du Plessis and Masliyah* [1991] suggests that $h^2/k_w = [9(1-\eta_w)^{2/3}]/[\eta_w(1-(1-\eta_w)^{1/3})]$; where h (m) is a measure of the half width of the rectangle. Therefore, for a permeable medium with rectangular pore tubes, the enhancement factor R_{wave}^{rec} can be expressed as

$$R_{wave}^{rec} = \left[\frac{S_c^2}{945}\left(\frac{9}{\eta_w}\right)^3\frac{(1-\eta_w)^2}{\left(1-(1-\eta_w)^{1/3}\right)^3}\right]\left[k_w \Re^2\{\beta_w G_w(0)\}\right] \cdot \left[\frac{A_p^2(0)k_w^2}{\mu^2\nu^2}\right]. \quad (32)$$

[50] The perturbation amplitude, $A_{\chi_1}(0)$, can now be estimated by combining equations (31) and (32) with the definition $R = F_{wave}(0)/F_{diff}(0)$ and the expressions for $F_{diff}(0)$ and $F_{wave}(0)$ defined by equation (27).

$$A_{\chi_1}(0) = 4 f_{cs}\left[\frac{A_p(0)k_w}{\mu\nu}\right]\left[\frac{D_e}{\nu}\right]\left[k_w \Re\{\beta_w G_w(0)\}\frac{\partial \chi_0}{\partial z}(0)\right], \quad (33)$$

where f_{cs} is the tube-shape geometry factor from equations (31) and (32) as appropriate and $\frac{\partial \chi_0}{\partial z}(0)$ is the vertical gradient of $\chi_0(z)$ at $z = 0$. Providing that $|F_{sd}| \ll F_{gd}$ (see Table 1), then the above formulations for R and $A_{\chi_1}(0)$ are formally the same as for the nondispersive case, except that the Schmidt number must now account for enhancement of diffusivity by the dispersion coefficient, i.e., $S_c = \nu/(D + \mathcal{D})$.

[51] Results of model simulations of a snowpack overlying an isothermal soil undergoing high- and low-frequency oscillatory pressure forcing are listed in Tables 1 and 2. Included in these tables are the component CO_2 fluxes, the amplitudes of the CO_2 wave, $A_{\chi_1}(0)$, predicted using equation (33), and the source term, S_χ, predicted using equation (16) or its equivalent in the case of a dispersive medium. The simulations with the source term in the upper model layer are not shown because they do not offer any information beyond that contained in Tables 1 and 2, except that all fluxes, other than $F_{sd}(0)$, are approximately twice those shown in Table 1.

[52] The results presented in these tables suggest that (1) $F_{wave}(0)$ increases with increasing frequency for both dispersive and nondispersive media, (2) $F_{wave}(0)$ is negligible for very low frequency (barometric) pressure forcing for either type of media, (3) $F_{wave}(0)$ decreases with increasing dispersivity of the medium, (4) when all other things are equal, $F_{wave}(0)$ is greater for media with pore tubes of rectangular cross section than those with cylindrical cross section, (5) because of $F_{gd}(0)$ oscillatory flow in a dispersive media can significantly enhance and even dominate $F_{diff}(0)$, and (6) F_{sd} is usually small compared to F_{gd}, but that it does become relatively more important at higher frequencies.

[53] Results shown in Table 1 also indicate that $F_{wave}(0)$ induced by high-frequency turbulent atmospheric pressure forcing does not contribute much to the overall fluxes. However, this conclusion does not necessarily extend to all possible situations for two reasons. The first can be seen from the enhancement factor, equations (31) and (32), which increases as the cube of permeability. Therefore $F_{wave}(0)$ is likely to be significantly higher for soils and snowpacks with permeabilities exceeding $k_w = 6.25 \times 10^{-9}$ m^2, which was used for this study. Second, atmospheric turbulence occurs on more than just one frequency. A more appropriate approach would relate the enhancement factor

Table 2. Model CO_2 Wave Amplitudes for Pore Tubes With Cylindrical ($A_{\chi 1}^{cyc}(0)$ (ppm)) and Rectangular ($A_{\chi 1}^{rec}(0)$ (ppm)) Cross Sections and CO_2 Source Terms, S_χ (ppm s^{-1}), Associated With the Fluxes Shown in Table 1

Frequency	Nondispersive			Dispersive		
ω, s^{-1}	$A_{\chi 1}^{cyc}(0)$	$A_{\chi 1}^{rec}(0)$	S_χ	$A_{\chi 1}^{cyc}(0)$	$A_{\chi 1}^{rec}(0)$	S_χ
1.0×10^{-5}	0.85×10^{-10}	0.12×10^{-9}	0.17×10^{-1}	0.38×10^{-11}	0.24×10^{-10}	0.43×10^{-1}
5.2×10^{-3}	0.74×10^{-2}	0.10×10^{-1}	0.17×10^{-1}	0.20×10^{-3}	0.16×10^{-2}	0.38×10^{-1}

to an integral over all appropriate frequencies, i.e., $R \propto \int_{\omega_l}^{\omega_u} \Re^2\{\beta_w G_w(0)\}\ S_p(\omega)d\omega$; where $S_p(\omega)$ is the power spectral density for turbulent pressure fluctuations and ω_u and ω_l are the limits of integration. This integration was performed (numerically) in an effort to be more precise about R_{wave}, such that: (1) $S_p(\omega)$ is obtained from *Horst* [1997], (2) the total variance is assumed to be $0.5A_p^2(0)$ with $A_p(0)$ = 10 Pa as before, (3) neutral atmospheric stability is assumed, (4) Taylor's hypothesis is used to relate the horizontal wave number of the turbulence to its frequency (i.e., $k_h = \omega/u$ where u is the horizontal wind speed), (5) the frequency at which the maximum of the frequency weighted spectra occurs is 0.13 Hz as indicated from observations by *Massman et al.* [1997] (this parameter is needed to model $S_p(\omega)$ [cf. *Horst*, 1997]), (6) $\omega_l = 10^{-3}$ Hz corresponding to a period of about 100 min, and (7) ω_u = 13 Hz was chosen with the intention of assuring that $W_o \leq 1$ (for $W_o > 1$ [*Watson*, 1983] indicates that $F_{wave}(0) \rightarrow 0$ very quickly with increasing W_o). For a nondispersive medium with pore tubes of rectangular cross section the results of this integration indicate that R_{wave} increases with increasing wind speed, but that $R_{wave} < 0.002$ for $u < 20$ m s^{-1}. While these estimates are admittedly crude, they do nevertheless indicate that the value for the high-frequency $F_{wave}(0)$ shown in Table 1 may underestimate the true turbulence-driven $F_{wave}(0)$ by 1 or 2 orders of magnitude.

[54] Before closing this section, three other points need to be discussed. The first concerns an important implication of the dispersive model. The second concerns the consequences of the approximations to $\mathcal{D}$ and $\partial\mathcal{D}(z)/\partial z$ and the third suggests how the lower boundary condition of the CO_2 wave, $A_{\chi_1}(D_w)$, may reasonably be chosen if the upper boundary condition is obtained from equation (33).

[55] 1. The dispersive model developed in this study suggests that the enhancement of diffusive fluxes by induced advective fluxes should be proportional to the dispersion coefficient (equations (28) and (29)), which in turn is linearly proportional to the pressure forcing, $A_p(0)$. This is different from *Watson*'s [1983] model and the observations of *Joshi et al.* [1983], which suggest that the enhancement should increase as $A_p^2(0)$. Clearly, the magnitude of the dispersivity, α, and the amplitude of the pressure forcing dictate the relative importance of the different advective enhancements. Consequently, it may be possible to assess if wintertime (eddy covariance) CO_2 fluxes observed in natural environments contain evidence for the different types of flux enhancements [e.g., *Takagi et al.*, 2005].

[56] 2. Table 1 shows that as the driving frequency ω increases the relative importance of the shear-dispersive flux can increase significantly. In fact, $F_{sd}(0)$ can become dominant at high enough frequencies or wave numbers. Without disregarding this term altogether in equation (24) or changing the approximations to the term $\partial\mathcal{D}(z)/\partial z$, this constraint on $F_{sd}(0)$ would seem to limit the dispersive model to those frequencies and wave numbers less than or about equal to those used in this study.

[57] 3. The CO_2 profiles shown in section 6 assumed that $A_{\chi_1}(0)$ = 1 ppm and that $A_{\chi_1}(D_w)$ = 0.25 ppm. However, using the model with $A_{\chi_1}(0)$ given by equation (33) should require a more logically based estimate of $A_{\chi_1}(D_w)$. The elements of such a choice are contained in equation (33). A relatively simple scaling argument based on this equation yields: $A_{\chi_1}(D_w) = A_{\chi_1}(0)[|G_w(D_w)|/|G_w(0)|][\chi_0(D_w)/\chi_0(0)]$, where the term $[|G_w(D_w)|/|G_w(0)|]$ accounts for the decrease in the forcing strength with depth, while the term $[\chi_0(D_w)/\chi_0(0)]$ allows for the increasing amounts of CO_2 with depth.

8. Conclusions

[58] This study outlines a new two-layer analytical model describing CO_2 profiles and fluxes in permeable snowpacks and soils associated with advective flows forced by periodic pressure fluctuations at the upper surface of the substrate. The model assumes that each layer has uniform, but different, physical properties with a CO_2 source term located in either the upper or lower layer. The substrate pressure field is described by wave solution to the diffusion equation. The CO_2 response is decomposed into a steady state solution and a wave solution to the advective-diffusive equation. The wave portion of the CO_2 model does include the possibility of a resonance, which could cause numerical problems for substrates of very low permeability. The model is first developed for nondispersive substrates and then extended to dispersive substrates.

[59] For a nondispersive medium the diffusive CO_2 flux is enhanced by wave flux forced by pressure oscillations at the upper surface. For a dispersive medium the model also describes two additional fluxes, which are proportional to the dispersivity of the medium, the pressure forcing, and the structure of the substrate. These additional fluxes are of opposite sign, but the counterdiffusive flux, induced by vertical velocity shear near the surface of the substrate, tends to be negligible for all but very high frequencies and horizontal wave numbers. Otherwise, depending upon the dispersivity of the medium and the strength of the pressure forcing, the dispersive-diffusive flux can enhance the diffusive flux significantly. Interestingly, in a dispersive medium the wave portion of the flux enhancement tends to be reduced over what would occur in a nondispersive medium. This is a result of slight differences in the mean gradient of the CO_2 within the substrate and the Schmidt number used to describe the wave enhancement [*Watson*, 1983] between nondispersive and dispersive media. Modeling results also indicate that a substrate network of pore tubes with rectangular cross section allow for greater enhancement of diffusive fluxes than would the same network of tubes with cylindrical cross section. A simple method for estimating the amplitude of the CO_2 perturbation induced within the substrate by the oscillatory forcing is given in terms of the amplitude of the pressure forcing, the mean substrate gradient, and substrate properties. Finally, all other things remaining equal, a model sensitivity study indicated that locating the CO_2 source term in the upper layer generally enhanced the CO_2 profiles and fluxes significantly over the case with the source term located in the lower layer.

Appendix A

[60] This appendix describes a relatively fast, convergent, phase-preserving algorithm for implementing the fifth boundary condition on the mass transfer model, equation (14), at the interface between the two layers ($z = D_w$). This approach ensures that the model can be used (as is done in part 2 of this study) to estimate the phase of the solution at D_w. The present method does not affect the phase because it

uses only real numbers to scale the solution to a specified magnitude at the interface, denoted here as in the main text by $A_{\chi_1}(D_w)$. By specifying magnitude of the solution, $\chi_1(z)$, at $z = D_w$ this fifth boundary condition is stronger than simply requiring that the two solutions be continuous across the interface. This algorithm assumes the previously stated upper and lower boundary conditions and that the upper and lower layer solutions are matched at the interface between the two layers.

[61] 1. In Step 1, assume a value for the upper boundary condition, $A_{\chi_1}(0)$, and calculate the magnitude of the solution at D_w, $|\chi_1(D_w)|$.

[62] 2. In Step 2, calculate the ratio $A_{\chi_1}(D_w)/|\chi_1(D_w)|$ and divide the upper boundary condition $A_{\chi_1}(0)$ by this ratio.

[63] 3. In Step 3, use this ratio, $\frac{A_{\chi_1}(0)}{A_{\chi_1}(D_w)/|\chi_1(D_w)|}$, as a new upper boundary condition for the model and calculate a new solution for $\chi_1^{new}(z)$ and a new value for $|\chi_1^{new}(D_w)|$.

[64] 4. In Step 4, calculate the new ratio $A_{\chi_1}(D_w)/|\chi_1^{new}(D_w)|$ and multiply the new solution $\chi_1^{new}(z)$ by this new ratio.

[65] 5. In Step 5, from this newly scaled solution, $[A_{\chi_1}(D_w)/|\chi_1^{new}(D_w)|]\chi_1^{new}(z)$, check to see how close the scaled upper boundary condition, $A_{\chi_1}(0)[|\chi_1(D_w)|/|\chi_1^{new}(D_w)|]$, is to the original upper boundary condition, $A_{\chi_1}(0)$.

[66] 6. In Step 6, if the scaled upper boundary condition is within an acceptable level of tolerance, say 10^{-3} for example, then the scaled solution, $[A_{\chi_1}(D_w)/|\chi_1^{new}(D_w)|]\chi_1^{new}(z)$, is the final solution that incorporates the measured boundary condition, $A_{\chi_1}(D_w)$, at $z = D_w$. If not, then return to Step 2 and repeat until the level of tolerance has been achieved. (For the present study this tolerance level was usually achieved in four iterations.)

Notation

A_p Amplitude of pressure wave or perturbation field (A_p is a function of depth), Pa.

A_χ Amplitude of CO_2 wave or perturbation field (A_χ is a function of depth) (mol fraction: ppm, mol mol^{-1}).

$A^{\pm}$ Amplitude of generic upward (+) and downward (−) propagating waves.

a pore tube radius (assuming the pore space of the substrate are cylindrical tubes), m.

c CO_2 molar density, mol m^{-3}.

D Coefficient of diffusivity for binary gases (e.g., CO_2 in air), m^2 s^{-1}.

D_e Effective coefficient of diffusivity (e.g., CO_2 in air within a porous medium; D_e^w = upper layer, D_e^l = lower layer), m^2 s^{-1}.

D_w Depth of snow layer (upper layer of a two-layer permeable substrate), m.

D_l Depth of soil layer (lower layer of a two-layer permeable substrate), m.

D_s $= D_w + D_l$ (total depth of the permeable substrate), m.

$\underline{\mathcal{D}}$ Dispersion tensor (3 × 3 matrix), m^2 s^{-1}.

$\mathcal{D}$ Coefficient of dispersion (scalar equivalent of $\underline{\mathcal{D}}$: $\mathcal{D}_w$ = upper layer, $\mathcal{D}_l$ = lower layer), m^2 s^{-1}.

$F(z)$ Nondimensional complex-valued function describing variation of the pressure wave at a depth z within the substrate ($F_w(z)$ = upper layer; $F_l(z)$ = lower layer).

$\overline{F}_\chi(0)$ Total (CO_2) flux exiting the upper surface ($z = 0$) of the substrate, ppm m s^{-1}.

$F_{diff}(0)$ Diffusive component of $\overline{F}_\chi(0)$, ppm m s^{-1}.

$F_{wave}(0)$ Nondispersive pressure pumping component of $\overline{F}_\chi(0)$, ppm m s^{-1}.

$F_{gd}(0)$ Gradient-dispersive pressure pumping component of $\overline{F}_\chi(0)$, ppm m s^{-1}.

$F_{sd}(0)$ Shear-dispersive pressure pumping component of $\overline{F}_\chi(0)$, ppm m s^{-1}.

$\mathcal{F}$ Parameter associated with pore geometry and flow characteristics within the substrate, s^4 m^{-2}.

f_{sc} scaling factor (nondimensional generalization of $\mathcal{F}$).

$G(z)$ Nondimensional complex-valued function describing variation of the pressure wave at a depth z within the substrate ($G_w(z)$ = upper layer; $G_l(z)$ = lower layer).

$G(0)$ $= G_w(z = 0)$ (note $|G(0)|$ = magnitude of the complex number $G(0)$).

H_p (real-valued) attenuation depth of the surface pressure wave, m.

h pore tube half-width (assuming substrate pore space is composed of rectangular tubes), m.

h_1, h_2, h_3, h_4 complex-valued, secondary, model constants, ppm, mol mol^{-1}.

i $= \sqrt{-1}$.

$\hat{\mathbf{i}}, \hat{\mathbf{j}}, \hat{\mathbf{k}}$ unit vectors associated with the x, y, and z coordinates.

k air permeability of the substrate (k_w = upper layer; k_l = lower layer), m^2.

k_{wl} secondary complex-valued model variable related to k_w and k_l, m.

$\mathbf{k_h}$ two-dimensional horizontal wave number, m^{-1}.

k_h magnitude of $\mathbf{k_h}$, m^{-1}.

$\hat{\mathbf{k}}_\mathbf{h}$ (dimensionless) unit vector corresponding to $\mathbf{k_h}$ ($\hat{\mathbf{k}}_\mathbf{h} = \mathbf{k_h}/k_h$).

n subscript referring to the integer harmonic of the CO_2 wave within the substrate ($n = 1, 2, 3, \ldots$).

P_0 mean atmospheric background pressure, Pa.

p perturbation pressure field (assumed to be a traveling plane wave in the horizontal with a depth-dependent amplitude: $p(x, y, z, t) = A_p(z)e^{i(\omega t - \mathbf{k_h} \cdot \mathbf{r_h})}$], Pa.

$\mathbf{r_h}$ two-dimensional vector representing horizontal distance, m.

R Dimensionless diffusional enhancement factor (ratio of pressure pumping flux to diffusional flux; see $F_{diff}(0)$, $F_{wave}(0)$, $F_{gd}(0)$, and $F_{sd}(0)$ above).

S_χ substrate CO_2 source term, ppm m^{-3} s^{-1}.

$S_p(\omega)$ Power spectrum as a function of frequency, ω.

t time, s.

u horizontal atmospheric wind speed, m s^{-1}.

$\mathbf{v}$ three-dimensional Darcian velocity ($\mathbf{v_w}$ = upper layer, $\mathbf{v_l}$ = lower layer), m s^{-1}.

$\mathbf{v_x}$, $\mathbf{v_y}$, $\mathbf{v_z}$ x, y, and z vector components of $\mathbf{v}$, m s^{-1}.

v magnitude of $\mathbf{v}$ ($v = \sqrt{v_x^2 + v_y^2 + v_z^2}$), m s^{-1}.

x, y, z spatial coordinates, m.

α dispersivity of the permeable substrate (α_L = lateral dispersivity, α_T = transverse dispersivity), m.

β complex-valued attenuation coefficient associated with the substrate pressure wave (determined by the frequency and horizontal wave number of the pressure wave and the vertical structure of the substrate; β_w = upper layer, β_l = lower layer), m^{-1}.

γ refers to 3 different, complex-valued, secondary model constants, ppm, mol mol^{-1}.

η air-filled porosity of the substrate (η_w = upper layer, η_l = lower layer) (dimensionless).

κ_p pressure diffusivity [$\kappa_p = P_0 k/(\eta\mu)$], m^2 s^{-1}.

λ complex-valued attenuation coefficient associated with the substrate CO_2 wave (determined by the frequency and horizontal wave number of the pressure wave, the effective diffusivity and the tortuosity of the substrate, and the wave harmonic; λ_w = upper layer, λ_l = lower layer), m^{-1}.

μ dynamic viscosity of air, Pa s.

ν kinematic viscosity of air, m^2 s^{-1}.

σ_w dimensionless real-valued secondary variable related to D_e^w and $\mathcal{D}^w$.

τ tortuosity of the substrate (τ_w = upper layer, τ_l = lower layer) (dimensionless).

ϕ_{wl} dimensionless real-valued secondary variable related to τ and η.

χ Substrate CO_2 mol fraction (composed a steady state portion, $\chi_0(z)$, and a series of harmonic plane waves (perturbation fields), $\sum_{n=1}^{\infty} \chi_n(z) e^{ni(\omega t - \mathbf{k_h} \cdot \mathbf{r_h})}$), ppm, mol mol^{-1}.

$\overline{\chi}(0)$ Mean CO_2 mol fraction at the top surface of the upper layer of substrate, ppm, mol mol^{-1}.

$\overline{\chi}(D_w)$ Mean CO_2 mol fraction at the interface between the upper and lower substrate layers, ppm, mol mol^{-1}.

ω wave frequency, Hz, radians s^{-1}.

$\boldsymbol{\nabla}$ three-dimensional gradient operator.

$\boldsymbol{\nabla_h}$ two-dimensional horizontal gradient operator.

∇^2 Laplacian operator.

[67] **Acknowledgments.** I would like to thank Andrew Altevogt, Gerhard Dangelmayr, Bob Hamre, Dick Sommerfeld, and Gene Takle for their scientific, mathematical, and editorial contributions to this manuscript. My thanks also to Mary Albert, Michael Novak, and Thomas Neumann for courageously agreeing to read this manuscript and for providing many helpful suggestions for making this study more readable and user friendly.

References

Albert, M. R., and J. P. Hardy (1995), Ventilation effects in a seasonal snow cover, in *Biogeochemistry of Seasonally Snow-Covered Catchments*, edited by K. A. Tonnessen et al., *IAHS Publ.*, *228*, 71–79.

Albert, M. R., and W. R. McGilvary (1992), Thermal effects due to air flow and vapor transport in dry snow, *J. Glaciol.*, *38*, 273–281.

Albert, M. R., E. F. Schultz, and F. E. Perron Jr. (2000), Snow and firn permeability at Stiple Dome, *Antarctica, Ann. Glaciol.*, *31*, 353–356.

Auer, L. H., N. D. Rosenberg, K. H. Birdsell, and E. M. Whitney (1996), The effects of barometric pumping on contaminant transport, *J. Contam. Hydrol.*, *24*, 145–166.

Bear, J. (1972), *Dynamics of Fluids in Porous Media*, Elsevier, New York.

Buckingham, E. (1904), Contributions to our knowledge of aeration of soils, *Bull. 25*, Bur. of Soils, U.S. Dep. of Agric., Washington, D. C.

Chatwin, P. C. (1975), On the longitudinal dispersion of a passive contaminant in oscillatory flows in tubes, *J. Fluid Mech.*, *71*, 513–537.

Clarke, G. K. C., and E. D. Waddington (1991), A three-dimensional theory of wind pumping, *J. Glaciol.*, *37*, 89–96.

Colbeck, S. C. (1989), Air movement in snow due to windpumping, *J. Glaciol.*, *35*, 209–213.

Cunningham, J., and E. D. Waddington (1993), Air flow and dry deposition of non-sea-salt sulfates in polar firn: Paleoclimate implications, *Atmos. Environ., Part A*, *27*, 2943–2956.

Du Plessis, J. P., and J. H. Masliyah (1991), Flow through isotropic granular porous media, *Transp. Porous Media*, *6*, 207–221.

Freeze, R. A., and J. A. Cherry (1979), *Groundwater*, Prentice-Hall, Upper Saddle River, N. J.

Fukuda, H. (1955), Air and vapor movement in soil due to wind gustiness, *Soil Sci.*, *79*, 249–256.

Gelhar, L. W., C. Welty, and K. R. Rehfeldt (1992), A critical review of data on field-scale dispersion in aquifers, *Water Resour. Res.*, *28*, 1955–1974.

Gjessing, Y. T. (1977), The filtering effects of snow, in *Isotopes and Impurities in Snow and Ice Symposium*, *IASH-AISH Publ.*, vol. 118, pp. 199–203, Bartholomew, Dorking, U. K.

Grivet-Talocia, S., F. Einaudi, W. L. Clark, R. D. Dennet, G. D. Nastrom, and T. E. vanZandt (1999), A 4-yr climatology of pressure disturbances using a barometer network in central Illinois, *Mon. Weather Rev.*, *127*, 1613–1629.

Harrison, W. D., D. Musgrave, and W. S. Reeburgh (1983), A wave-induced transport process in marine sediments, *J. Geophys. Res.*, *88*, 7617–7622.

Hauf, T., U. Finke, J. Neisser, G. Bull, and J.-P. Strangenberg (1996), A ground-based network for atmospheric pressure fluctuations, *J. Atmos. Oceanic Technol.*, *13*, 1001–1023.

Horst, T. W. (1997), A simple formula for attenuation of eddy fluxes measured with first-order-response scalar sensors, *Boundary Layer Meteorol.*, *82*, 219–233.

Huettel, M., and I. T. Webster (2001), Porewater flow in permeable sediments, in *The Benthic Boundary Layer*, edited by B. P. Bourdreau and B. B. Jørgensen, pp. 144–179, Oxford Univ. Press, New York.

Jiao, J. J., and H. Li (2004), Breathing of coastal vadose zone induced by sea level fluctuations, *Geophys. Res. Lett.*, *31*, L11502, doi:10.1029/2004GL019572.

Joshi, C. H., R. D. Kamm, J. M. Drazen, and A. S. Slutsky (1983), An experimental study of gas exchange in laminar oscillatory flow, *J. Fluid Mech.*, *133*, 245–254.

Karam, M. A. (2000), A thermal wave approach for heat transfer in a nonuniform soil, *Soil Sci. Soc. Am. J.*, *64*, 1219–1225.

Katul, G. G., J. D. Albertson, C.-I. Hsieh, P. S. Conklin, J. T. Sigmon, M. B. Parlange, and K. R. Knoerr (1997), The "inactive" eddy motion and the large-scale turbulent pressure fluctuations in the dynamic sublayer, *J. Atmos. Sci.*, *53*, 2512–2524.

Labolle, E. M., and G. E. Fogg (2001), Role of molecular diffusion in contaminant migration and recovery in an alluvial aquifer system, *Transp. Porous Media*, *42*, 155–179.

Lee, X., and A. G. Barr (1998), Climatology of gravity waves in a forest, *Q. J. R. Meteorol. Soc.*, *124*, 1403–1419.

Lewicki, J. L., W. C. Evans, G. E. Hilley, M. L. Sorey, J. D. Rogie, and S. L. Brantley (2003), Shallow soil CO_2 flow along the San Andreas and Calaveras Faults, California, *J. Geophys. Res.*, *108*(B4), 2187, doi:10.1029/2002JB002141.

Lichtner, P. C., S. Kellar, and B. Robinson (2002), New form of dispersion tensor for axisymmetric porous media with implementation in particle tracking, *Water Resour. Res.*, *38*(8), 1146, doi:10.1029/2000WR000100.

Massman, W. J., and J. M. Frank (2006), Advective transport of CO_2 in permeable media induced by atmospheric pressure fluctuations: 2. Observational evidence under snowpacks, *J. Geophys. Res.*, *111*, G03005, doi:10.1029/2006JG000164.

Massman, W. J., R. A. Sommerfeld, R. A. Mosier, K. F. Zeller, T. J. Hehn, and S. G. Rochelle (1997), A model investigation of turbulence-driven pressure-pumping effects on the rate of diffusion of CO_2, N_2O, and CH_4, through layered snowpacks, *J. Geophys. Res.*, *102*, 18,851–18,863.

Massmann, J., and D. F. Farrier (1992), Effects of atmospheric pressure on gas transport in the vadose zone, *Water Resour. Res.*, *28*, 777–791.

Nappo, C. J. (2002), *An Introduction to Atmospheric Gravity Waves*, Elsevier, New York.

Nilson, R. H., E. W. Peterson, K. H. Lie, N. R. Burkhard, and J. R. Hearst (1991), Atmospheric pumping: A mechanism causing vertical transport of contaminated gases through fractured permeable medium, *J. Geophys. Res.*, *96*, 21,933–21,984.

Perfect, E. (2003), A pedotransfer function for predicting solute dispersivity: Model testing and upscaling, in *Scaling Methods in Soil Physics*, edited by Y. Pachepsky et al., pp. 89–96, CRC Press, Boca Raton, Fla.

Rees, J., P. S. Anderson, and J. C. King (1998), Observations of solitary waves in the stable atmospheric boundary layer, *Boundary Layer Meteorol.*, *86*, 47–61.

Robinson, A. L., R. G. Sextro, and W. J. Fisk (1997), Soil-gas entry into an experimental basement driven by atmospheric pressure fluctuations — Measurements, spectral analysis, and model comparison, *Atmos. Environ.*, *31*, 1477–1485.

Saffman, P. G. (1960), Dispersion due to molecular diffusion and macroscopic mixing through a network of capillaries, *J. Fluid Mech.*, *7*, 194–208.

Scotter, D. R., and P. A. C. Raats (1968), Dispersion of water vapor in soil due to air turbulence, *Soil Sci.*, *108*, 170–176.

Severinghaus, J. P., R. F. Keeling, B. R. Miller, R. F. Weiss, B. Deck, and W. S. Broecker (1997), Feasibility of using sand dunes as archives of old air, *J. Geophys. Res.*, *102*, 16,783–16,792.

Sommerfeld, R. A., W. J. Massman, and R. C. Musselman (1996), Diffusional CO_2 flux through snow: Spatial and temporal variability among alpine-subalpine sites, *Global Biogeochem. Cycles*, *10*, 473–482.

Takagi, K., M. Nomura, D. Ashiya, H. Takahashi, K. Sasa, Y. Fujinuma, H. Shibata, Y. Akibayashi, and T. Koike (2005), Dynamic carbon dioxide exchange through snowpack by wind-driven mass transfer in a conifer-broadleaf mixed forest in northernmost Japan, *Global Biogeochem. Cycles*, *19*, GB2012, doi:10.1029/2004GB002272.

Waddington, E. D., J. Cunningham, and S. L. Harder (1996), The effects of snow ventilation on chemical concentrations, in *Chemical Exchange Between the Atmosphere and Polar Snow*, edited by E. W. Wolff and R. C. Bales, pp. 403–451, Springer, New York.

Watanabe, T. (2004), Large-eddy simulation of coherent turbulent structures associated with scalar ramps over plant canopies, *Boundary Layer Meteorol.*, *112*, 307–341.

Watson, E. J. (1983), Diffusion in oscillatory pipe flow, *J. Fluid Mech.*, *133*, 233–244.

Webster, I. T. (2003), Wave enhancement of diffusivities within surficial sediments, *Environ. Fluid Mech.*, *3*, 269–288.

Webster, I. T., and J. H. Taylor (1992), Rotational dispersion in porous media due to fluctuating flow, *Water Resour. Res.*, *28*, 109–119.

W. J. Massman, Rocky Mountain Research Station, USDA Forest Service, 240 West Prospect, Fort Collins, CO 80526, USA. (wmassman@fs.fed.us)